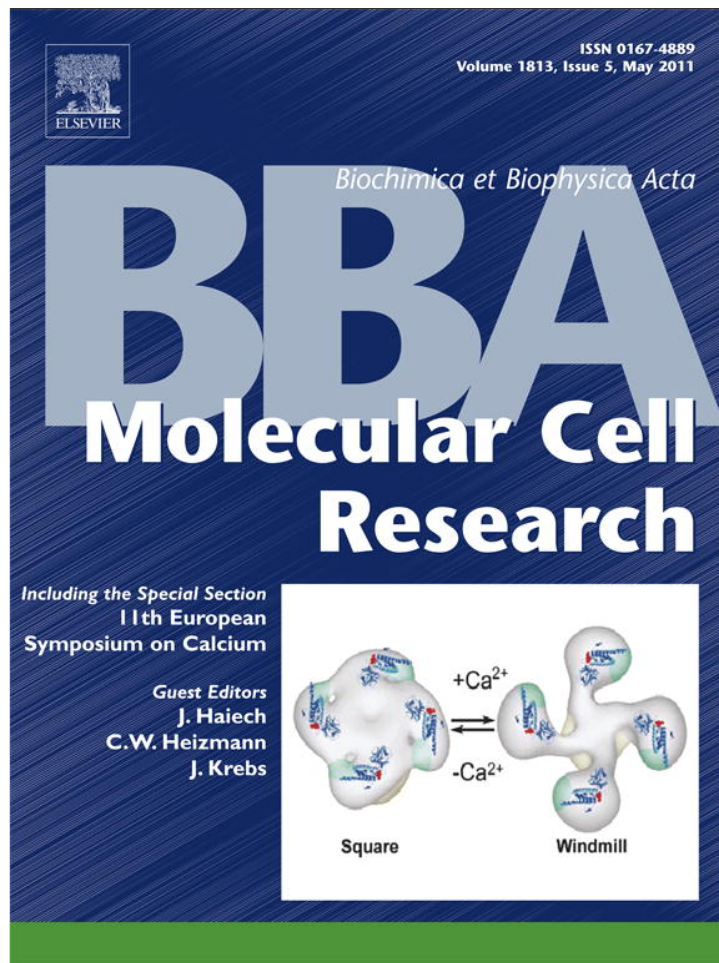


Provided for non-commercial research and education use.
Not for reproduction, distribution or commercial use.



This article appeared in a journal published by Elsevier. The attached copy is furnished to the author for internal non-commercial research and education use, including for instruction at the authors institution and sharing with colleagues.

Other uses, including reproduction and distribution, or selling or licensing copies, or posting to personal, institutional or third party websites are prohibited.

In most cases authors are permitted to post their version of the article (e.g. in Word or Tex form) to their personal website or institutional repository. Authors requiring further information regarding Elsevier's archiving and manuscript policies are encouraged to visit:

<http://www.elsevier.com/copyright>



Contents lists available at ScienceDirect

Biochimica et Biophysica Acta

journal homepage: www.elsevier.com/locate/bbamcrSingle actomyosin motor interactions in skeletal muscle[☆]Zeno Földes-Papp^{a,b,c,*}, Shih-Chu Jeff Liao^b, Ben Barbieri^b, Karol Gryczynski Jr.^{a,d}, Rafal Luchowski^a, Zygmont Gryczynski^a, Ignacy Gryczynski^a, Julian Borejdo^a, Tiefeng You^b^a Department of Molecular Biology and Immunology, University of North Texas Health Science Center, 3500 Camp Bowie Boulevard, Fort Worth, TX 76107, USA^b ISS, 1602 Newton Drive, Champaign, IL 61822, USA^c Medical University of Graz, Department of Internal Medicine, Division of Clinical Angiology, A-8036 Graz, Austria^d Department of Physics, University of North Texas, Denton, TX, USA

ARTICLE INFO

Article history:

Received 9 November 2010

Received in revised form 23 December 2010

Accepted 1 February 2011

Available online 21 February 2011

Keywords:

Single actomyosin

Live skeletal muscle cell

Polarization dependent fluorescence fluctuations

Time-dependent photon distributions

Molecular orientations

ABSTRACT

We present a study of intramuscular motion during contraction of skeletal muscle myofibrils. Myofibrillar actin was labeled with fluorescent dye so that the ratio of fluorescently labeled to unlabeled protein was 1:10⁵. Such sparse labeling assured that there was on average only one actin-marker present in the focus at a given time. From the intensity signal in the two orthogonal detection channels, significant fluctuations, similar to fluorescent burst in diffusion-based single-molecule detection schemes, were identified via a threshold algorithm and analyzed with respect to their intensity and polarization. When only rigor complexes were formed, the fluctuations of polarized intensity were characterized by unimodal Gaussian photon distributions. During contraction, in contrast, bimodal Gaussian photon distributions were observed above the rigor background threshold. This suggests that the bimodal Gaussian photon distributions represent pre- and post-power stroke conformations. Clusters of polarized photons indicated an anisotropy decay of single actomyosin motors of ~9 s during muscle contraction. This article is part of a Special Issue entitled: 11th European Symposium on Calcium.

© 2011 Elsevier B.V. All rights reserved.

1. Introduction

The basic cellular function of myosin motor is to deliver ATP-dependent force impulses to the rope-like actin polymer. Upon binding of ATP, the myosin head detaches from an old binding site on actin, reattaches to a new actin monomer, and when ATP is hydrolyzed changes conformation causing sliding of actin with respect to myosin [1]. In the experiments presented in this study we labeled actin in skeletal muscle myofibril with 0.1 nM rhodamine-phalloidin (RP) plus 10 μM unlabeled phalloidin (UP), i.e. only one in 10⁵ molecules was fluorescently labeled. Since the observable volume (ΔV_{obs}) of confocal microscope is ~10⁻¹⁵ L, there is on average only one fluorescent molecule in the ΔV_{obs} at any time, and the Poissonian probability of detecting more than one labeled actin-marker within the focus of the laser beam was negligible. The green cylinder in Fig. 1 represents the volume illuminated by the laser. Diameter of the cylinder, $2\omega_0$, is equal to the diameter of the confocal pinhole (50 μm) divided by the magnification of the objective (40×) and is 1.2 μm. The ΔV_{obs} has height z_0 , equal to the thickness of a typical myofibril. Taking this thickness as

1 μm, $\Delta V_{\text{obs}} = \pi\omega_0^2 z_0 = 1 \mu\text{m}^3$ (alternatively, the volume is often taken as an ellipsoid of revolution with the volume $4/3\pi\omega_0^2 z_0$). This is approximately equal to the volume of a half-sarcomere; indeed, the length, width and height of a typical half-sarcomere (HS) are 1, 1, and 0.5 μm, respectively and therefore its volume ~1 μm³ (10⁻¹⁵ L). Thus, the signal detected by the instrument is contributed only by the fluorescent molecules in one half-sarcomere. This number can be calculated by realizing that the concentration of actin in muscle is as high as 0.6 mM [2]. Therefore, there are ~60,000 actin protomers in one HS. Recall that the myofibril was labeled with 0.1 nM fluorescent phalloidin plus 10 μM unlabeled phalloidin, so only one in 100,000 actin protomers carried fluorescent phalloidin. Thus, the calculation gives 1 fluorescent actin in the HS = ΔV_{obs} .

In rigor muscle, thin filaments are immobilized by strongly bound cross-bridges (left panel in Fig. 1), a fluorophore (red dot) never changes orientation or leaves the ΔV_{obs} and, consequently, autocorrelation is flat (bottom left). The situation is different during contraction (right panel). Here the interaction of cross-bridges with thin filament is expected to cause a fluorophore to continuously change orientation. Since the fluorophore is illuminated by linearly polarized light, the amount of light it absorbs (and re-emits) is dependent on instantaneous orientation. Moreover, the fluorescent actin-marker may leave and re-enter the ΔV_{obs} as the cross-bridges pull filaments to the left, and filaments recoil during isometric contraction to the right. Fluorescence intensity oscillates and autocorrelation function is non-zero, as illustrated at the bottom right in Fig. 1.

[☆] This article is part of a Special Issue entitled: 11th European Symposium on Calcium.

* Corresponding author at: Department of Molecular Biology and Immunology, University of North Texas Health Science Center, 3500 Camp Bowie Boulevard, Fort Worth, TX 76107, USA.

E-mail addresses: Zeno.Foldes-Papp@medunigraz.at, zeno.foldespapp@gmail.com (Z. Földes-Papp).

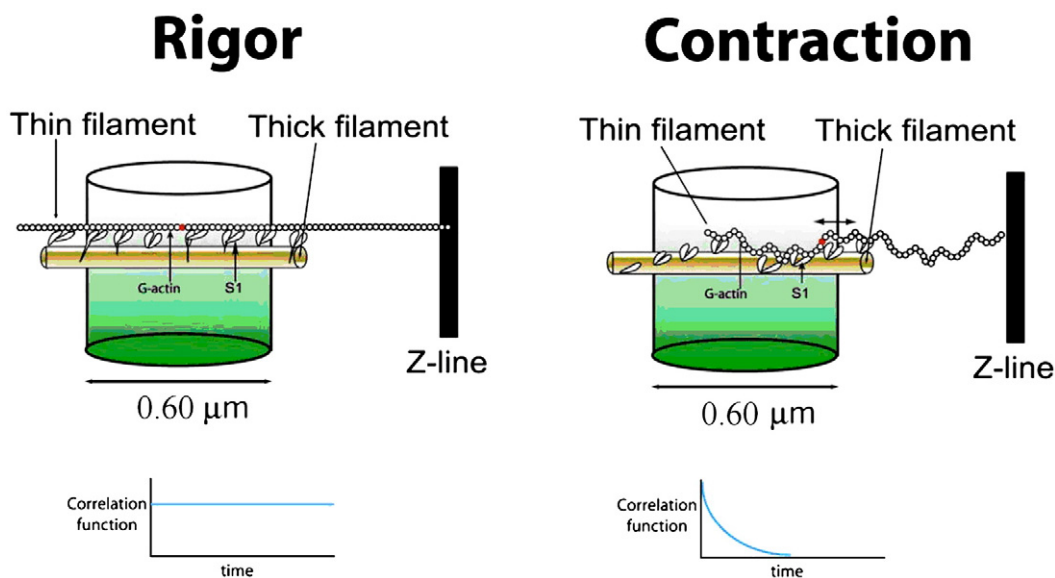


Fig. 1. Schematic representation of the experiments at different states of muscle fluorophore. A single actin in a sarcomere is labeled with a fluorophore (red). Its fluorescence in the detection observational volume ΔV_{obs} (green cylinder) is measured for a few seconds. In rigor fluorescence remains constant and autocorrelation function of fluctuations is flat (left panel). In contraction, the force impulses delivered by cross-bridges to thin filament deform actin filament, changing the orientation of a transition dipole of rhodamine rigidly attached to actin protomer. As a result, the intensity of polarized fluorescence of rhodamine fluctuates in time. In addition, fluctuations arise because rhodamine may leave and re-enter ΔV_{obs} as cross-bridges pull filaments to the left, and filaments recoil during isometric contraction to the right. The molecule is pulled to the left by the contractile force and recoils after pulled by isometric load to the right (right panel). Autocorrelation function is non-zero. See text for details.

The aim of this work was to study dynamic behavior of single actomyosin complexes during contraction in living skeletal muscle. The method presented resembles the procedures used in single-molecule spectroscopy, where significant events are separated from the background by means of intensity thresholding and then analyzed by probability density function to reveal subpopulations. Under contraction conditions, all single actomyosin motor molecules studied revealed skewed time-dependent photon distributions in two orthogonal polarization detection channels, which were fitted by two Gaussians. In contrast, all rigor photons were distributed unimodal Gaussian.

2. Materials and methods

2.1. Chemicals and solutions

Rhodamine-phalloidin (RP) was from Invitrogen (Carlsbad, CA). All other chemicals including 1-ethyl-3-(3'-dimethylaminopropyl) carbodiimide (EDC), dithiothreitol (DTT), creatine phosphate and creatine kinase were from Sigma. EDTA-rigor solution contained 50 mM KCl, 2 mM EDTA, 1 mM DTT, and 10 mM Tris-HCl buffer pH 7.5. Ca-rigor, contracting and relaxing solutions were as described earlier [3].

2.2. Preparation of myofibrils

Psoas muscles from 6-month-old white New Zealand rabbits were used. Thin strips of glycerinated muscle were incubated in EDTA-rigor solution until they turned white (~1 h). The fiber bundle was then homogenized using a Heidolph Silent Crusher S homogenizer for 20 s (with a break to cool after 10 s) in Mg^{2+} -rigor solution.

2.3. Sample preparation

Myofibrils were freshly prepared for each experiment. Myofibrils (1 mg/mL) (~4 μM actin) were mixed with 0.1 nM rhodamine-phalloidin plus 10 μM unlabeled phalloidin. Unlabeled phalloidin was necessary to prevent uneven labeling. If it was not there, the

sarcomeres closest to the tip of the pipette used to add the label would have contained more chromophores than sarcomeres further away from the tip. The degree of labeling was 10 μM /0.1 nM = 100,000, i.e. on the average one actin protomer in 10^5 was fluorescently labeled. Labeled myofibrils (25 μl) were applied to a coverslip (Menzel-Glaser 20 \times 20 mm #1 or Corning #1 25 \times 60 mm). The sample was left on a coverslip for 3 min to allow the myofibrils to adhere to the glass. The bottom cover slip was covered with a small coverslip (to prevent drying) and the two were separated by Avery Hole Reinforcement Stickers. Labeled myofibrils were washed with 5 volumes of the Ca^{2+} -rigor solution by applying the solution to the one end of the channel and absorbing with #1 filter paper at the other end.

2.4. Cross-linking

Myofibrils irreversibly shorten in contracting solution. To prevent the shortening the myofibrils (1 mg/mL) were incubated with 20 mM EDC for 10 min at room temperature according to procedure of Herrmann et al. [4]. The reaction was stopped by 20 mM DTT. Cross-linking did not affect ATPase. The lack of shortening was checked by comparing the length of DIC image of a myofibril before and 100 s after inducing contraction. Within the limits of measuring accuracy on the computer screen (~1%), the length always remained unchanged. Cross-linked myofibrils are a good model for muscle fiber ATPase and the kinetics of Ca^{2+} -activated activity [5]. The large $P(i)$ bursts and k_{cat} values were the same in cross-linked myofibrils and muscle fibers [4]. Those results were confirmed by Lionne et al. [6].

2.5. ATPase measurements

Myofibrillar suspension (200 μl of 1 mg/mL) was incubated in 0.1 mM ATP for 30, 60, 90 and 120 s. After the specified time, the reaction was stopped by 700 μl of 1 mM HCl. The samples were filtered through a cotton ball in a 1 mL pipette tip. Malachite Green (MG) reagent (100 μl) from the SensoLyte Phosphatase assay kit (AnaSpec, San Jose, CA) was added and incubated for 5 min. Phosphate (10 μl) contained in the kit was dissolved in 190 μl of deionized water along with 700 μl HCl and 100 μl MG reagent and

used as a standard. Standard (1 mL of 10 μM) contained 10^{-9} moles of phosphorus. The concentration of phosphate was measured at 650 nm. Ca^{2+} -rigor (200 μL) containing 700 μL HCl and 100 μL MG reagent was used as a blank. $[\text{P}_i]$ was calculated as $\text{mol}/1 \text{ mol}/\text{min} = \text{Abs}(\text{sample}) [\text{standard mol}]/\text{Abs}(\text{standard})/[\text{myosin mol}]/\text{min}$. The amount of myosin in 200 μL of 1 mg/mL myofibrils was taken as 0.2×10^{-9} mol. The mean \pm SD of 4 measurements were $3.1 \pm 0.8 \text{ s}^{-1}$, which is a first order chemical rate constant characterizing the ATPase activity of the myofibrils for the combination of substrate with the enzyme at low ATP concentrations. Obviously in the case of the reaction discussed here, so long the ATP (substrate) concentration was much lower than the Michaelis constant using the actual concentrations during the catalysis, the plot of initial velocity against ATP concentration gave a straight line.

2.6. Data collection in live muscle cells by a two-channel ALBA fluorescence fluctuation spectrometer and imaging system

The experiments were performed using a two-channel Alba-FCS (ISS, Champaign, IL) confocal system coupled to Olympus IX 71 microscope. The objective was water immersion NA = 1.15, 40 \times . The excitation was by a 532-nm cw-laser, and the observation was through a 550-nm long pass filter. The confocal pinhole was 50 μm . The laser was polarized vertically. The myofibrils were also vertical on the microscope stage. Inside the ALBA system, orthogonally linearly polarized analyzers (polarizing filters) were placed before each single-photon counting avalanche photodiodes (APD Mod SPCM-AQR-1S, Perkin-Elmer, Vaudereuil, Canada). The emitted fluorescence of channel 1 (Ch1) and channel 2 (Ch2) was separately focused on the APD's as shown in Fig. 2. Fluorescence data points were collected every 10 ms for 20 s.

2.7. Computational procedures and data analysis of photon streams

From the intensity signal in two polarization selective detection channels, significant fluctuations, similar to fluorescent bursts in diffusion-based single detection schemes, were identified by the novel analysis procedure, termed the Fluctuation Analyzer TZ with respect to their intensity and polarization (see Fig. 3). From the observed asymmetry in the distribution function, we inferred clear differences between the fluctuations under rigor conditions and contraction conditions. All contraction data showed the presence of additional dynamic modes in the orientation motion of actin filaments above the rigor fluctuations in intensity signal in two polarization selective detection channels (see Figs. 4 and 5). Since we studied intramuscular motion during contraction of skeletal muscle myofibrils, all rigor fluctuations were considered as 'background' and subtracted from the contraction data. By means of intensity thresholding as it resembles the procedures used in standard single-molecule spectroscopy, significant events were separated from the background and then analyzed by a histogram or probability density function to reveal subpopulations. The choice of the threshold level had no effect on the statistics of the fluctuation analysis as we demonstrate in Figs. 4 and 5. The fluctuation statistics of the actomyosin behavior was not distorted by this approach, but for clarity of presentations we subtracted rigor fluctuations in contraction data.

This work presents a study of the dynamics of skeletal muscle myofibrils using a novel fluorescence fluctuation spectroscopy approach. Specifically, raw photon count data from each channel were collected using Vista software (ISS, Champaign, IL). The data were exported for analysis with the software program, the TZ Fluctuation Analyzer, developed at ISS. Briefly, the collected

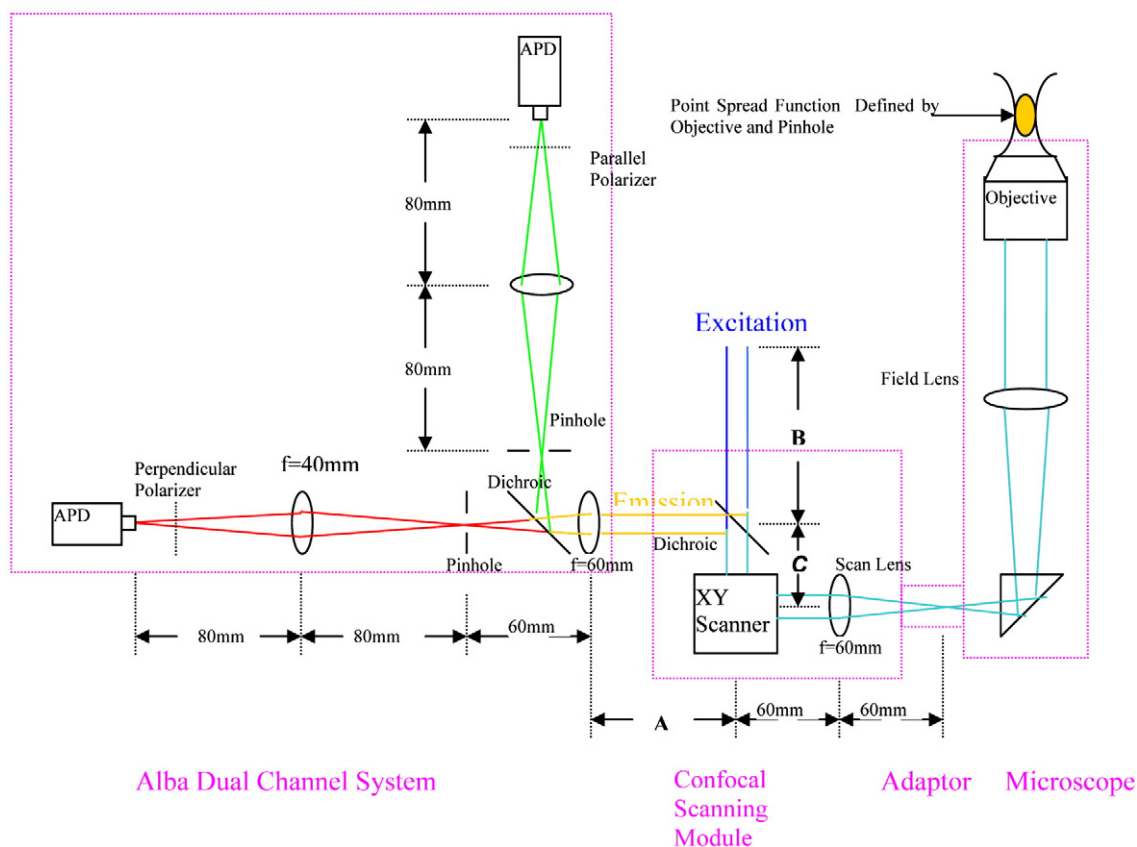


Fig. 2. ISS dual channel FCS and Confocal image system with scanning mirrors. The optical setup was used in this single-molecule study of fluorescently labeled actin-markers that are immobilized by attachment to myofibrils (thick filaments) in the living skeletal muscle cell.

fluorescence photon stream data are analyzed by calculating the correlation function (FCS) or photon counts distribution (PCH). The TZ Fluctuation Analyzer analyzes the photon stream data uniquely by looking for photon counts fluctuations. Given the fluorescence photon stream data as input, in the format of photon counts for each time bin, the Fluctuation Analyzer first searches for the peak-like characteristics in the data, where photon counts increase and then decrease. If the photon counts at the local maximum are above a certain threshold level, the software considers it as a fluctuation and saves the time position and photon counts of the local maximum. The Fluctuation Analyzer also saves the time position of the start and the end of each peak shape. Once the search of fluctuations is completed, the time position and intensity values of the found fluctuations can be further analyzed for statistics of the fluctuations, e.g., distribution of number of fluctuations over measurement time, distribution of number of fluctuations over photon counts, and distribution of number of fluctuations over time-in-between fluctuations (off-times). From those distributions, one can calculate the probability function and probability density function of the fluctuations. To fit the observed distributions with theoretical models, both linear regression and non-linear regression routines are implemented in the software.

When the photon stream data are collected with two detection channels and polarizing filters (polarizers, see subsection “Data collection in live muscle cells by a two-channel ALBA Fluorescence Fluctuation Spectrometer and Imaging System,” the software searches for fluctuations in each channel, and provides the option of calculating the polarization and anisotropy for fluctuations when they occur in both channels simultaneously. The fluctuations can be further analyzed for distributions. We also corrected the polarization and anisotropy values, respectively, for the numerical aperture of the objective $NA = 1.15$ (the effective aperture was even smaller for the excitation) and the refractive index inside muscle cells as analyzed by Axelrod [7]. However, the corrections only varied on average by 3.47% over the data points of a measurement, e.g. over 546 data points. Therefore, we use uncorrected time-dependent data.

We present frequency curves of photon events by binned histograms. Binned histograms of photons and continuous variate photon populations are not depicting the same information. In the histograms, the area of each bin (box) is proportional to the frequency which, in this case, is the number of measured polarization dependent fluorescence fluctuations within a given bin (box)-width. Instead of the frequency f_1 of a variate value X_1 as in a box of a histogram, we also considered the frequency of variate values in a narrow strip lying between x and $x + dx$. This frequency is $f(x)dx$. The frequency of variate values that lie anywhere between $x = a$ and $x = b$ is the integral $\int_{x=a}^b f(x)dx$. Then, the total frequency, i.e. the total number of individual fluctuations in the distribution, was $\int_{x=1}^g f(x)dx$. The probability that an individual fluctuation selected at random had a variate value between x and $x + dx$ was equal to the portion of the total frequency with a variate value between x and $x + dx$. This proportion was $\frac{f(x)dx}{\int_{x=1}^g f(x)dx} = p(x)$. The quantity $p(x)$ is the probability density function of the photon distribution. It was analogous to the $p_1 = f_1 / (f_1 + f_2 + \dots + f_n)$ of a countable (finite) photon distribution consisting of f_1 individual fluctuations with variate value X_1 , of f_2 with variate value X_2 and so on up to f_n with variate value X_n . Continuous populations of photon events have simple formulas, which enable properties to be calculated simply and quickly.

The polarized fluorescence intensity fluctuations are spread out along all intensity regions. By means of intensity thresh-holding, significant events were separated from the background to reveal subpopulations. Because the overall photon count in contraction data was about 2-fold greater than in rigor data we did not have to apply a linear transformation (operator) between data vector spaces in order to preserve the operation of data vector addition in the original data. Even though we implemented a linear operator for data transformation into the software package Fluctuation Analyzer TZ, we were able

to simply subtract the rigor fluctuations from contraction data without changing the statistics of preferred orientational motion of actin filaments under contraction conditions.

2.8. Testing of association between anisotropy and time in subset of photons showing slow dynamic relaxation behavior in actomyosin motors

We used the linear regression model to measure the association between anisotropy and time. R^2 is the squared product-moment correlation coefficient r , also called Pearson's r . The higher the values of R^2 , the better the agreement between measured data points and the theoretical curves. We can allow for the possibility that the number n of data points is small ($n < 10$) by testing the significance of a non-zero values of r : $t = r \sqrt{\frac{n-2}{1-R^2}}$, which is distributed approximately as Student's distribution with $\nu = n - 2$ degrees of freedom, does not depend on the original distribution of the anisotropy and time values. The decision criterion reads: $|t| \geq t_{\alpha, \nu} \rightarrow H_0$ rejected, where $1 - \alpha$ is the significant level (confidence interval) for the rejection of no correlation H_0 between anisotropy and time in the subset of polarized photons. The test is one-tailed because significance is only indicated if r is negative.

2.9. Measuring anisotropy in solution

Fluorescence anisotropies in solutions were measured by time-domain technique using FluoTime 200 fluorometer (PicoQuant GmbH, Berlin, Germany). The excitation was by a 475-nm pulsed laser diode, and the observation was through a monochromator at 590 nm with a supporting 590-nm long wave pass filter. The FWHM of pulse response function was 68 ps. Time resolution was better than 10 ps. The intensity decays were analyzed in terms of a multi-exponential model using FluoFit software (PicoQuant GmbH).

2.10. Rotation of rhodamine-phalloidin bound to F-actin

We checked that the measured orientation of the transition dipole of the fluorophore reflects the orientation of the protein. To this end, we compared anisotropy of RP with the anisotropy of RP bound to F-actin. The decay of the anisotropy of RP was best fitted by a single exponent in which 100% of the signal was contributed by the decay time of 0.519 ns. This is consistent with the rotation of a molecule of $M_w = 1250$. No independent rotation of rhodamine moiety was observed. The best fit of the decay of anisotropy of RP bound to thin filaments was bi-exponential with correlation times of 0.665 and 36.8 ns. The relative contributions were 13.7 and 86.3%, respectively. The short correlation time is due to the rotation of rhodamine-phalloidin and the long one to the rotation of F-actin oligomers. Thus over 86% of fluorescent phalloidin is immobilized by F-actin.

2.11. Notation

Following the original notation of Tregear and Mendelson [8], the first and second subscripts in the polarized intensity indicate the direction of excitation and emission polarization with respect to the laboratory frame of reference. Myofibrils were always vertical with respect to the laboratory frame of reference. For example I_{VV} indicates that the myofibril was illuminated with vertically polarized light (parallel to the axis of muscle) and that the intensity was detected through a polarizer oriented vertically (parallel to the axis of the muscle).

3. Results

The orientations of the reporter dye within the single actomyosin motor in working skeletal muscle cells (Fig. 1) were measured by

fluorescence polarization confocal microscopy (Fig. 2). We used single-molecule detection to study the time-dependence of molecular orientation of the actomyosin motor molecules. Fig. 3 depicts representative fluorescence fluctuation time series of a single actomyosin motor under rigor and contraction conditions. By applying vertically polarized exciting light V at 532-nm and detecting the emission components vertically $VV(t) = \text{Ch 2}$ (pink), and horizontally polarized, $VV(t) = \text{Ch 1}$ (blue), the fluorophore transition dipole on actin emitted a time-dependent, spatially anisotropic polarized signal collected by the two-channel polarization-sensitive optical system. $VV(t)$ and $VV(t)$ were recorded under identical experimental conditions except for the emission polarizing settings. The fluctuations differed in the magnitude and number. The total emitted fluorescence of the signal is obtained by adding the counts of both polarization channels for joint polarized intensity fluctuations. Ch1 + Ch2 (black) represent the most probable parameter value in the

sense that the probability of observing counts is the highest. We shall find explicit expression for likelihood functions which make Ch1 + Ch2 a maximum to compare the intensity of the signal between different trajectories. From the intensity signal in two polarization selective detection channels Ch1 and Ch2, the polarization values of intensity fluctuations were obtained (green).

Fig. 4 shows the histogram of measured time-dependent polarized fluorescence intensity fluctuations of that molecule under rigor condition. The binned histogram with the frequency of photon events in a bin (box) provides a better idea of how the photon events vary inside bins. We describe the probability of finding fluctuations in terms of a probability distribution which gives the probability of finding the fluctuation at various approximate polarized fluorescence intensities. A unimodal Gaussian photon distribution was obtained with the following parameter values in good agreement with the experimental observations of the frequency versus photon counts plot of Fig. 4: maximum intensity value 7.816 ± 0.695 KHz, $\chi^2 = 2.054 \times 10^{-3}$. Under contraction condition, the molecule also had a sufficiently strong central tendency as depicted in Fig. 5 with the first and second central moments of $\mu = 14.088$ KHz and $\sqrt{\mu_2} = 1.836$ KHz, but the measured photon distribution was skewed with $\beta_1 = 2.635$. β_1 Values are simple powers of the first few semi-invariants of the centered moments, i.e. $\beta_1 = \mu_3^2 / \mu_2^3$ and characterizes the shape of the distribution. β_1 signified a measured photon distribution with an asymmetric tail extending out towards more positive variate values. The skewed shape of the photon distribution was best fitted by a trimodal Gaussian distribution with the following parameter values: first maximum intensity value 10.041 ± 0.660 KHz, second maximum intensity value 13.850 ± 1.956 KHz, third maximum intensity value 19.661 ± 0.380 KHz, $\chi^2 = 2.657 \times 10^{-3}$. The trimodal fit was overly accurate. χ^2 values for the one- and two-modal fits were less accurate and strengthen the argument for choosing three populations. The trimodal character of Fig. 5 depended on the differences in fluorescence fluctuations with respect to intensity and polarization between Figs. 4 (rigor condition) and 5 (contraction condition). Our analysis is based on different muscle preparations and performed at different dates. We obtained the differences between rigor and contraction conditions in all muscle preparations but we depict in Figs. 4 and 5 only one. The differences were statistically significant. The additional two modes above rigor (see Fig. 5) under contraction conditions were significantly greater by magnitude (photon counts) and numbers. The overall photon count in Fig. 5 was about 2-fold greater than in Fig. 4 due to additional dynamic modes in the orientational motion of actin filaments under contraction conditions. Choosing three populations and the χ^2 values for the seemingly less accurate one- and two modes was reproducible in all data analyzed (for additional explanations see subsection 2.7. Computational procedures and data analysis of photon streams, first paragraph). Thus, we could simply subtract the rigor fluctuations from contraction data without changing the statistics of preferred orientational motion

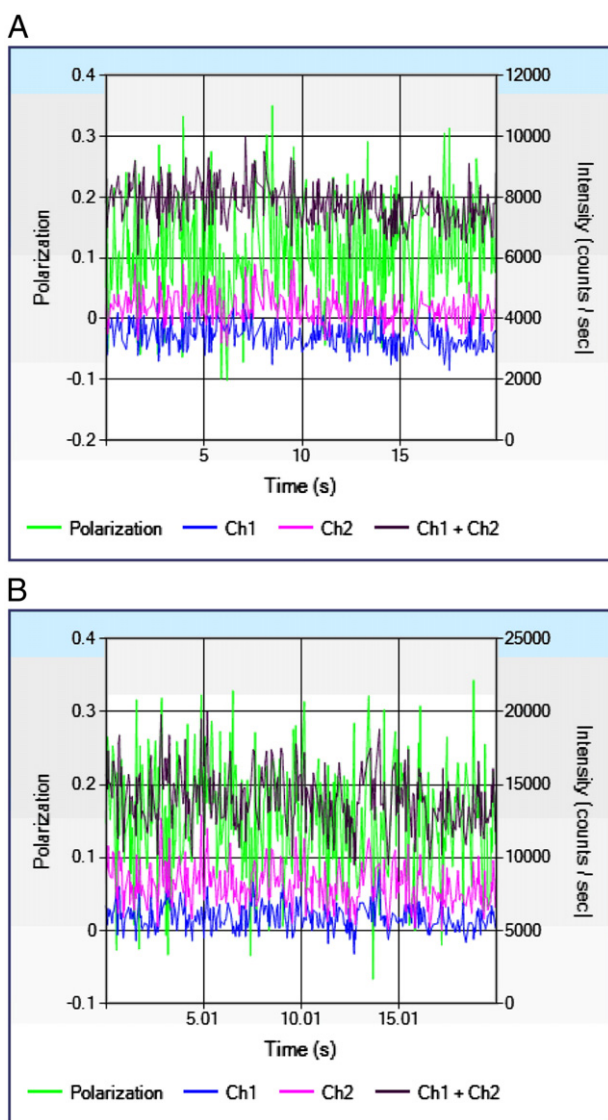


Fig. 3. Fluorescence fluctuation time series of a single actomyosin motor under rigor and contraction conditions. See text for details. (A) Experimental rigor condition of a single actomyosin motor in a skeletal muscle cell. Three hundred and twenty-five fluctuations in Ch1 (channel 1) and Ch2 (channel 2) were measured as function of time. The maximum magnitude of fluctuations was 5 KHz in Ch1, and it was 6.4 KHz in Ch2. (B) Experimental contraction condition of a single actomyosin motor in a live skeletal muscle cell as function of time. Three hundred and fifty-one fluctuations in channel 1 (Ch1) and channel 2 (Ch2) were measured. The maximum magnitude of fluctuations was 9.1 KHz in Ch1, and it was 12.7 KHz in Ch2.

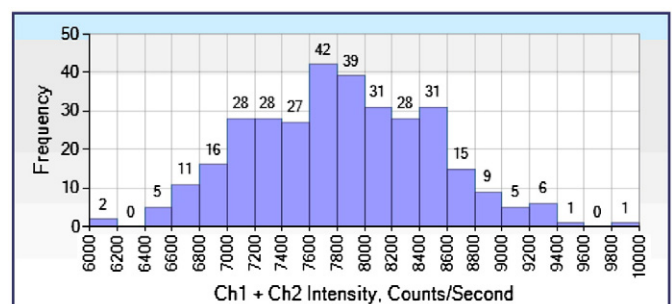


Fig. 4. Experimental rigor condition of a single actomyosin motor in a live skeletal muscle cell. Histogram of measured time-dependent polarized fluorescence intensity fluctuations.

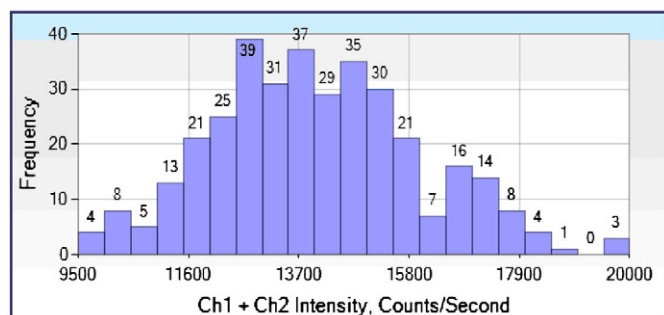


Fig. 5. Experimental contraction condition of a single actomyosin motor in a live skeletal muscle cell. Histogram of measured time-dependent polarized fluorescence intensity fluctuations.

of actin filaments under contraction. We did not apply a linear transformation (operator) between data vector spaces in order to preserve the operation of data vector addition in the original data.

The synopsis of analyzed single actomyosin motor molecules under rigor and contraction conditions is shown in Table 1. Under contraction conditions all single actomyosin motor molecules revealed skewed time-dependent photon distributions, whereas all rigor photon distributions were unimodal Gaussian. The rigor signal is contributed by immobile chromophores and therefore is treated here as background. Even though the unimodal rigor modes are of little interest in this study, they were present in large numbers under contraction conditions, and they always yielded the first intensity maximum of the trimodal Gaussian photon distributions under contraction. An appropriate approach was subtracting the rigor background noise in contraction data.

Fig. 6A shows the histogram of measured time-dependent polarized fluorescence intensity fluctuations above the rigor background threshold of 5.0 KHz in Ch1 and 6.4 KHz in Ch2 for that particular motor molecule under contraction. A bimodal Gaussian photon distribution was obtained in very good agreement with experimental observations of the frequency versus photon counts plots with the following parameter values: first maximum intensity value 14.264 ± 1.665 KHz, second maximum intensity value 19.923 ± 0.183 KHz. This finding has never been demonstrated before. Since the overall photon count in the measured contraction data was about 2-fold greater than in rigor data, there were enough high count rate data points that contributed to the analysis by subtraction the rigor modes from contraction data. This has the advantage of presenting a ready picture of single actin contraction activity without common

Table 1

Synopsis of characteristic parameters of measured time-dependent photon distributions of single actomyosin motors in live muscle cells.

Different single actomyosin motor molecules under the experimental conditions of rigor and contraction	Central moments		Skewness parameter $\beta_1 = \mu_3^2 / \mu_2^3$
	μ in Hz	$\sqrt{\mu_2}$ in Hz	
No. 1 under rigor	7954	± 451	n.a.
No. 1 under contraction	7595	± 3718	2.28
No. 2 under rigor	8379	± 691	0.04
No. 2 under contraction	9536	± 3981	0.96
No. 3 under rigor	5121	± 581	0.08
No. 3 under contraction	7607	± 3491	4.14
No. 4 under rigor	5590	± 583	n.a.
No. 4 under contraction	8782	± 3986	1.62
No. 5 under rigor	5364	± 593	0.19
No. 5 under contraction	10607	± 4504	1.81
No. 6 under rigor	5408	± 404	n.a.
No. 6 under contraction	6989	± 2758	1.64

n.a.: not applicable because of an experimental outlier value. However, the distribution was still best represented by a unimodal Gaussian photon distribution.

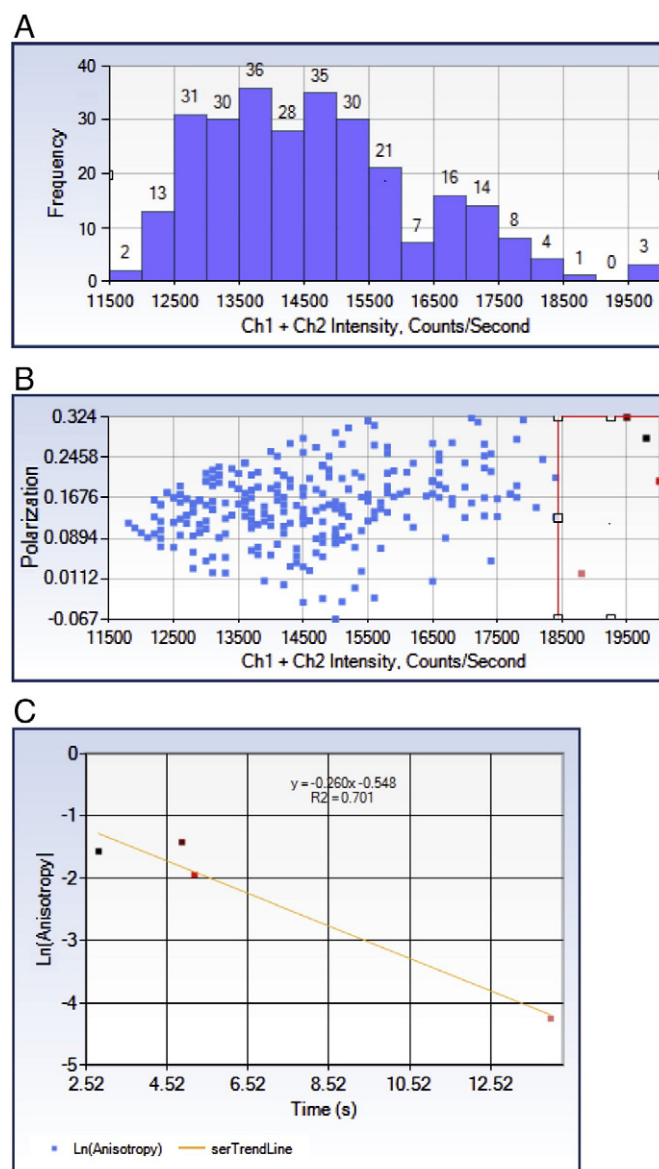
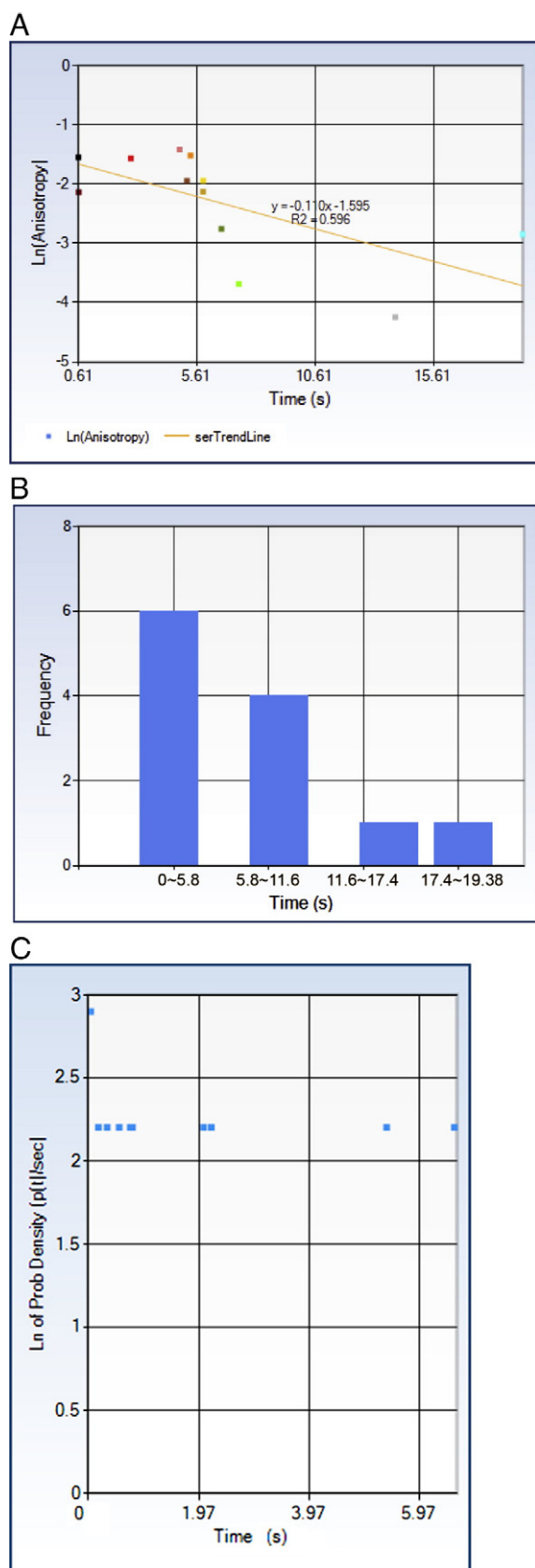


Fig. 6. Measured time-dependent polarized fluorescence intensity fluctuations above the rigor background threshold of 5.0 KHz in channel 1 and 6.4 KHz in channel 2 of single actomyosin motor molecule. (A) Histogram of polarized photon counts emitted by the single actomyosin motor molecule. (B) Correlation plot between time-dependent polarization and total photon counts emitted by the single actomyosin motor molecule under contraction conditions. The framed photon counts correspond to the second Gaussian photon distribution in (A) and is further quantified in (C). (C) Subset of photon distribution in (A) and (B) showing a slow dynamic relaxation behavior of the emission anisotropy. The regression curve was found for the pairs of related observations, i.e. for anisotropy and time.

molecular background ‘noise’ originating from rigor modes in contraction data during measurements. The structural and functional reason for this is that we found an equal amount of well-defined orientational background fluctuations (rigor modes of orientational modes) of single actomyosin motor molecules.

Next, we analyzed polarization above rigor noise. The polarization P followed the in-plan orientation of the emission dipole moment of the actomyosin complex. P values of -1 indicated a molecular orientation along the 90° direction, i.e. the emitted light was totally polarized in the perpendicular direction and perpendicular to the axis of myofibrils, whereas P values of $+1$ meant a molecular orientation along the 0° direction, i.e. the emission of the single dipole was completely polarized in the parallel direction and the electric vector of the exciting light was totally maintained parallel to the axis of the

myofibril. In Fig. 6B, the framed cluster between Ch1 and Ch2 intensity minimum of 18.429 KHz and maximum of 20.062 KHz indicated an additional dynamic relaxation process with intercept of -0.548 in the photon subset (Fig. 6C) corresponding to an anisotropy $A_0 = 0.578$



which differed from the measured average anisotropy of 0.111. This curve in Fig. 6C gives more concise information about the relation between the variable anisotropy and time than the whole set of data itself (Figs. 6A and B). It is important to note that only the variable anisotropy is subject to scatter, whereas time could be controlled precisely. The quantitative measure of how closely the two variables are related is R^2 and r , respectively (see 2. Materials and methods, subsection 2.8. “Testing of association between anisotropy and time in subset of photons showing slow dynamic relaxation behavior in actomyosin motors”). Under the reasonable assumption that r is distributed approximately normally, we found the association between anisotropy and time $|t = -2.17| \geq t_{\alpha=0.125; \nu=2} = 1.60 \rightarrow H_0$ rejected with a significance level of 87.5%. The problem we addressed in live-cell approach was timescale separation in the dynamics of single actomyosin motors, which occurred when one form of dynamics is much slower than another. To this end, long measurement times of at least 20 s needed to allow evolution of the slower modes. This was especially useful if fast rigor modes are not of interest in themselves and, therefore, were subtracted in the contraction time series. Under experimental contraction conditions, a proper quantification was possible by averaging over single actomyosin motor molecules.

Fig. 7 presents the average outcome of six actomyosin motor molecules. In rigor muscle cell, the orientation of the actomyosin motor is fixed and, therefore, we could not observe the slow dynamics under rigor conditions. In contrast, in contraction muscle cell, the orientation of the actomyosin motor is variable. Thus, the emission anisotropy was observed as a function of time in the subset of photons showing the slow dynamics $A(t) = A_0 \cdot e^{-t/\tau}$, in which A_0 is the anisotropy at the beginning of contraction function and τ is the correlation time (Fig. 7A). The plot of $\ln(A)$ versus t is linear and has a slope of -0.110 per second. The strength of the association is $|t = -3.84| \geq t_{\alpha=0.005; \nu=10} = 3.17 \rightarrow H_0$ rejected with a significance level of 99.5%. Thus, we found a correlation time of the slow dynamic process in the actomyosin motors of $\tau = 9.09$ s (with $A_0 = 0.203$). The dynamics that falls into the subset of photons depicted in Fig. 7A was further characterized by its time-dependent fluctuation number distribution in Fig. 7B, and its fluctuation off-time distribution in Fig. 7C. Interestingly, the slow relaxation dynamics revealed molecular memory as shown in Fig. 7C. We found that anisotropy in rigor and contraction is different because orientation is different in rigor and contracting muscle cell. In rigor muscle cell, the orientation is well defined. In contracting muscle cell, the orientation is variable. Because anisotropy is different, the polarized fluorescence intensities are different. We did not find molecular memory in rigor time traces.

4. Discussion

The myofibrils labeled with the ratio of fluorescently labeled to unlabeled actin-markers were chosen such that the estimated number of labeled actins present in the observation volume at a given time was equal or smaller than unity. The aim of this work was to study dynamic behavior of single actomyosin interaction complexes during contraction in live cells. This was accomplished through measurements of fluorescence polarization of actin labeled with rhodamine-

Fig. 7. Time-dependent polarized fluorescence intensity fluctuations above the biological rigor background noise in six actomyosin motor molecules under experimental contraction conditions. (A) Subset of photons showing the slow dynamic relaxation behavior of the emission anisotropy in actomyosin motors: minimum intensity (Ch1 + Ch2) = 15.082 KHz, maximum intensity (Ch1 + Ch2) = 81.170 KHz, average polarization 0.180, average anisotropy 0.130. (B) Fluctuation number distribution of the subset photons in (A). (C) The logarithmic probability density of off-times is plotted against the off-times. The off-times between the random fluctuations do not yield a negative exponential distribution that would give a line with a negative slope in the logarithmic probability density versus off-time plot. We measured a different behavior as depicted. Thus, the fluctuations in the photon subset of (A) occurred at random with molecular memory. For details see text.

phalloidin. The focus of previous experimental studies of actomyosin at the single-molecule level was mainly the cross-bridge attachment (power stroke) and detachment events of myosin to actin [9–14]. It is for this reason that in the present study we recorded dynamic processes in live skeletal cells by means of polarized fluorescence intensity time series. The fluorescence intensity fluctuations were detected through polarizers oriented vertically, i.e. parallel to the axis of muscle, and horizontally, i.e. perpendicular to the axis of muscle, by the two-channel optical system (Fig. 2). The time series were defined by the start time and the time resolution of the measurements (Fig. 3). The latter was 10 ms throughout this study.

First, the measured data of Figs. 4–6 are presented initially as binned frequency histograms which enable a qualitative inspection in panel A. The shapes of the histograms Figs. 4–6A are different. Only the data of Fig. 4 are distributed practically ‘symmetrically’ but the data of Figs. 5 and 6A are somewhat ‘skewed’. Certainly, skewness does not mean that the data lack sufficient accuracy and precision. It simply indicates the presence of additional modes (local maxima) in the data. We applied central moments characterizing the polarized fluorescence intensity signal in the two detection channels. Our finding that the contraction data showed intensity signals in two polarization-sensitive detection channels with the two mean maxima above the rigor fluctuations has major implications. From the observed asymmetry in the distribution function, we infer the presence of additional dynamic modes in the orientational motion of actin filaments under contraction conditions. The fact that contraction above rigor modes can be described by two Gaussian and rigor cannot is significant because it suggests that the two Gaussians represent pre- and post-power stroke conformations.

Second, the acquisition of photon distribution above biological rigor noise via our threshold algorithm became necessary because of the overlapping signals in time. For this reason the so-called correlation plot (Fig. 6B) of measured polarization versus total polarized fluorescence intensities (rigor background corrected) defined the region of interest, which corresponded to the second Gaussian photon distributions.

We think that a relaxation process shown in Fig. 7 represents slow decay of oscillations of a whole actin filament. Now, let us assume that the probability of being not active, i.e. not moving, is independent of how much time has previously passed. Therefore, the probability of non-active within an observation time interval, which we call time between two successive fluctuations ΔT measured in the polarized fluorescence time series, is linearly proportional to that time interval. Hence, we got

$$\text{Prob}\{\tau \in (t, t + \Delta T)\} = \alpha \cdot \Delta T, \quad (1)$$

where $\alpha = \text{const}$ here is a multiplier (proportionality factor). Because the fluctuations are random, it is possible that the actomyosin molecule spends a little bit longer in its non-active, non-moving states. For the single actomyosin molecule to still be non-active at time $t + \Delta T$, it has to be non-active at time t and during the time ΔT of its contraction fluctuations. The joint probability of both independent events was

$$S(t + \Delta T) = S(t) \cdot (1 - \alpha \cdot \Delta T). \quad (2)$$

S stands for still non-active. We can immediately write

$$\frac{S(t + \Delta T) - S(t)}{\Delta T} = -\alpha \cdot S(t). \quad (3)$$

We took the limit $\Delta T \rightarrow 0$ and obtained

$$\frac{dS}{dt} = -\alpha \cdot S(t). \quad (4)$$

Hence,

$$S(t) = e^{-\alpha \cdot t}. \quad (5)$$

Now, the theoretical probability density function of times between fluctuations $p_{\Delta T}(t)$ was given by

$$p_{\Delta T}(t) = -\frac{dS}{dt}. \quad (6)$$

From Eq. (6), we got

$$p_{\Delta T}(t) = \alpha \cdot e^{-\alpha \cdot \Delta T}. \quad (7)$$

The probability density function of times between fluctuations in the measured time series has units of time^{-1} (see also Fig. 7C). ΔT denotes the variate that occurs without molecular memory. Eq. (7) means that the intervals of time between the random happenings without molecular memory have a negative exponential distribution. In other words, it is much more likely to have short off-times ΔT in the measured fluorescence time series than long ones. α can have any value between 0 and infinity. The negative exponential distribution (7) is a reverse J-shaped distribution and the greater α the more sharply the distribution curve $p_{\Delta T}(t)$ slopes for $\Delta T \cong 0$. It has the following properties of the mean μ and the variance $\sigma^2 = \mu^2$

$$\mu = \frac{1}{\alpha}, \quad \mu_2 = \frac{1}{\alpha^2}, \quad (8)$$

so that the standard deviation equals $1/\alpha =$ the mean. To test whether the random process under study had no memory, i.e. $\alpha \neq \alpha(t)$, we compared the exponential decay of Eq. (7) with the measured probability densities $p_{\Delta T}(t)$ of times between successive fluctuations obtained from the measured polarized fluctuation time traces. By plotting $\ln p_{\Delta T}(t)$ versus ΔT in Fig. 7C, the off-times trajectories of fluctuations revealed a significant difference in behavior from Eq. (7), which cannot be caused by the negative exponential distribution of off-times (7). It is a fair deduction, then, that the subset of fluctuations in Fig. 7A do not strictly occur at random. We found a merely alternative way of the off-time distribution that is a memory effect, in which an individual actomyosin molecule repeats similar behavior suggesting that structural features are somehow remembered during contraction functions.

In summary, in Fig. 7C, we found a new measure of contraction fluctuations above random background orientation in the rigor fluorescence time series. We were able to sort out molecular noise and drifts (e.g. photobleaching) from contraction fluctuations. We call this measure ‘molecular memory’. The comparison of the fluorescence signal obtained from corresponding rigor data revealed that molecular memory was not present in rigor data.

5. Conclusions

The presented methodology represents a significant application of a novel single-molecule fluctuation approach to an important biological problem. Rhodamine-labeled phalloidin was mixed with unlabelled phalloidin at a ratio of $\sim 1:100,000$ and added to myofibrils irreversibly shortened with contracting solution and cross-linked with EDC. Single-molecule detection was used to study the time-dependence of molecular orientation of the actomyosin motor molecules under rigor and contraction conditions. In this way the cross-bridge attachment (power stroke) and detachment events of myosin to actin was followed. Specifically, the emitted fluorescence was collected using two channels to view simultaneously the parallel or perpendicular component. The collected fluorescence photon stream data were analyzed by a novel analysis procedure, termed the Fluctuation Analyzer TZ. We searched for the peak-like characteristics in the data, where photon counts increased and then decreased.

If the photon counts at the local maximum were above a certain threshold level, the software considered it as a fluctuation and saved the time position and photon counts of the local maximum. The Fluctuation Analyzer also saves the time position of the start and the end of each peak shape. The contraction data obtained was explained by two Gaussian photon distributions of on-average orientations that represented the mean maxima pre- and post-power stroke conformations. The clusters of polarized photons indicated an anisotropy decay of single actomyosin motors of ~9 s during muscle contraction. Thus, the ability to interact using different orientations of the reporter dipole on actin was an important feature of the single actomyosin molecules in skeletal muscle myofibrils.

Acknowledgments

This work was supported by Austrian FWF grant P20454-N13 (Z.F.-P.), NIH grants R01EB12003 and 5R21CA14897 (Z.G.), and by NIH grant 1R01-HL090786 (J.B.). Z.F.P. received visiting professorships at the Department of Molecular Biology and Immunology, University of North Texas Health Science Center and at ISS (Champaign, IL).

References

- [1] M.A. Geeves, K.C. Holmes, Structural mechanism of muscle contraction, *Ann. Rev. Biochem.* 68 (1999) 687–728.
- [2] C.R. Bagshaw, *Muscle contraction*, Chapman & Hall, London, 1982.
- [3] P. Muthu, N. Calander, I. Gryczynski, Z. Gryczynski, J.M. Talent, T. Shtoyko, I. Akopova, J. Borejdo, Monolayers of silver nanoparticles decrease photobleaching: application to muscle myofibrils, *Biophys. J.* 59 (2008) 3429–3438.
- [4] C. Herrmann, J. Sleep, P. Chaussepied, F. Travers, T. Barman, A structural and kinetic study on myofibrils prevented from shortening by chemical cross-linking, *Biochemistry* 32 (1993) 7255–7263.
- [5] C. Herrmann, C. Lionne, F. Travers, T. Barman, Correlation of ActoS1, myofibrillar, and muscle fiber ATPases, *Biochemistry* 33 (1994) 4148–4154.
- [6] C. Lionne, B. Iorga, R. Candau, F. Travers, Why choose myofibrils to study muscle myosin ATPase? *J. Muscle Res. Cell Motil.* 24 (2003) 139–148.
- [7] D. Axelrod, Carbocyanine dye orientation in red cell membrane studied by microscopic fluorescence polarization, *Biophys. J.* 26 (1979) 557–573.
- [8] R.T. Tregear, R.A. Mendelson, Polarization from a helix of fluorophores and its relation to that obtained from muscle, *Biophys. J.* 15 (1975) 455–467.
- [9] J.S. Spudich, S.J. Kron, M.P. Sheetz, Movement of myosin-coated beads on oriented filaments reconstituted from purified actin, *Nature* 315 (1985) 584–586.
- [10] K. Kitamura, M. Tokunaga, A.H. Iwane, T. Yanagida, A single myosin head moves along an actin filament with regular steps of 5.3 nanometers, *Nature* 397 (1999) 129–134.
- [11] M.A. Geeves, K.C. Holmes, Structural mechanism of muscle contraction, *Ann. Rev. Biochem.* 68 (1999) 687–728.
- [12] J.N. Forkey, M.E. Quinlan, M.A. Shaw, J.E.T. Corrie, Y.E. Goldman, Three-dimensional structural dynamics of myosin V by single-molecule fluorescence polarization, *Nature* 422 (2003) 399–404.
- [13] A. Yildiz, J.N. Forkey, S.A. McKinney, T. Ha, Y.E. Goldman, P.R. Selvin, Myosin V walks hand-over-hand: single fluorophore imaging with 1.5-nm localization, *Science* 300 (2003) 2061–2065.
- [14] S. Syed, G.E. Snyder, C. Franzini-Armstrong, P.R. Selvin, Y.E. Goldman, Adaptability of myosin V studied by simultaneous detection of position and orientation, *EMBO J.* 25 (2006) 1795–1803.